


# Transformation of L-DOPA and Dopamine on the Surface of Gold Nanoparticles: An NMR and Computational Study

Nikolina Kalčec, Antonio Ljulj, Lucija Božičević, Valerije Vrček, Domenico Marson, Sabrina Pricl, Frances Separovic, and Ivana Vinković Vrček\*

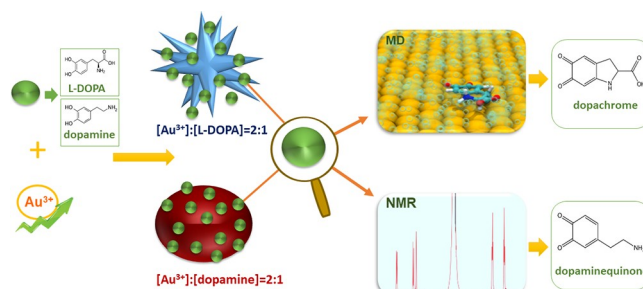
ACCESS |

 Metrics & More

 Article Recommendations

 Supporting Information

**ABSTRACT:** Gold nanoparticles (AuNPs) have found applications in biomedicine as diagnostic tools, but extensive research efforts have been also directed toward their development as more efficient drug delivery agents. The high specific surface area of AuNPs may provide dense loading of molecules like catechols (L-DOPA and dopamine) on nanosurfaces, enabling functionalization strategies for advancing conventional therapy and diagnostic approaches of neurodegenerative diseases. Despite numerous well-described procedures in the literature for preparation of different AuNPs, possible transformation and structural changes of surface functionalization agents have not been considered thoroughly. As a case in point, the catechols L-DOPA and dopamine were selected because of their susceptibility to oxidation, cyclization, and polymerization. To assess the fate of coating and functionalization agents during the preparation of AuNPs or interaction at the nano–bio interface, a combination of spectroscopy, light scattering, and microscopy techniques was used while structural information and reaction mechanism were obtained by NMR in combination with computational tools. The results revealed that the final form of catechol on the AuNP nanosurface depends on the molar ratio of Au used for AuNP preparation. A large molar excess of L-DOPA or dopamine is needed to prepare AuNPs functionalized with fully reduced catechols. In the case of molar excess of Au, the oxidation of catechols to dopamine quinone and dopaquinone was promoted, and dopaquinone underwent intramolecular cyclization in which additional oxidation products, leukodopachrome, dopachrome, or its tautomer, were formed because of the larger intrinsic acidity of the more nucleophilic amino group in dopaquinone. MD simulations showed that, of the oxidation products, dopachrome had the highest affinity for binding to the AuNPs surface. The results highlight how a more versatile methodological approach, combining experimental and *in silico* techniques, allows more reliable characterization of binding events at the surface of AuNPs for possible applications in biomedicine.



## INTRODUCTION

Gold nanoparticles (AuNPs) have been increasingly used in the design and development of advanced biomedical products including drug delivery formulations and biosensors.<sup>1</sup> The high specific surface area of AuNPs enables dense loading and adsorption of different molecules, paving the way for advanced theranostic strategies using a plethora of surface functionalization possibilities.<sup>2</sup> Excellent optical and adsorption properties of AuNPs have been combined with different aptamers for label-free colorimetric sensing.<sup>3,4</sup> Thus, different biosensing strategies based on AuNPs have been developed for detecting the important catechols, dopamine, and L-DOPA.<sup>3,5–9</sup> Functionalization of AuNPs with various agents has been also proposed as brain-targeting and drug-delivery strategies for treatment of neurodegenerative diseases.<sup>10,11</sup> Catechols may be used not only as a surface coating but also as reducing agents for the preparation of functionalized AuNPs. However, catechols may undergo oxidation in the presence of gold salt.<sup>7,12–17</sup>

Different transformation patterns at the nano–bio interface should be considered, including cyclization, polymerization, and so on. The AuNP–catechol interaction was used in this study as a model system to demonstrate the importance of novel methodological approaches for assessing the fate of biomolecules at the nanosurface. The work was based on the AuNP functionalization strategies with dopamine and L-DOPA published recently.<sup>13</sup>

While most scientific literature on novel functionalization strategies of nanomaterials describes the use of techniques based on electron microscopy, light scattering, electrochemistry, calorimetry, UV–vis, or fluorescence spectroscopy,

there is a considerable lack of structural information obtained by nuclear magnetic resonance (NMR) spectroscopy. Additionally, comprehensive experimental characterization combined with computational tools may give deeper insight into complex mechanisms occurring at the nanosurface. A similar approach, as was recently published for mechanistic evaluation of the interaction between metallic NPs and biothiols, was applied.<sup>18</sup> We obtained mechanistic data, thus providing valuable evidence-based knowledge and a solid basis for facilitating the complex design of nanoenabled medical products.

## ■ MATERIALS AND METHODS

**Chemicals and Reagents.** All chemicals were purchased from Sigma-Aldrich Chemie GmbH (Munich, Germany) unless specified otherwise and were used without further purification. Trisodium citrate dihydrate (CIT) was obtained from Alfa Aesar (Kandel, Germany). Before use, all glassware and stir bars were cleaned with aqua regia (HCl:HNO<sub>3</sub>, 3:1 v/v) and rinsed with ultrapure water (UPW).

**Synthesis and Characterization of AuNPs in the Presence of L-DOPA and Dopamine.** AuNPs were prepared in two steps as described previously,<sup>13</sup> with some modifications. In the first step, 14 nm spherical citrate-coated AuNP seed (citAuNPs) was prepared by the chemical reduction of HAuCl<sub>4</sub> by CIT at 100 °C. Briefly, 11.8 mg of HAuCl<sub>4</sub>·3H<sub>2</sub>O was dissolved in 100 mL of ultrapure water (UPW) and heated under reflux with constant stirring. When the solution was brought to boil, 300 μL of 388 mM CIT was rapidly added. The reaction was allowed to proceed for 30 min until the solution attained a wine-red color. citAuNPs were then cooled and kept at 4 °C in the dark until further use.

Different molar ratios of catechols and HAuCl<sub>4</sub> were tested to design catechol-functionalized AuNPs (see Table S1 in the Supporting Information). Experiments were based on mixing 100 μL of 0.1 M HAuCl<sub>4</sub>·3H<sub>2</sub>O, 144 μL of 0.38 mM citAuNPs, 400 μL of 1.7 mM methoxypoly(ethylene glycol) (mPEG) thiol, and 4 mL of different molar concentrations of L-DOPA or dopamine hydrochloride in a total volume of 50 mL under vigorous stirring. The concentration of HAuCl<sub>4</sub> was kept constant, while the concentration of L-DOPA and dopamine was adjusted. After 2 h of stirring, obtained catechol-coated AuNPs were pelleted by centrifugation at 800g for 10 min and kept at 4 °C in the dark.

The mass concentration of Au in AuNPs suspensions was determined by a graphite furnace atomic absorption spectrometer (GFAAS) (PerkinElmer AAnalyst 600, PerkinElmer, Shelton, USA) by using Au standard solution (1000 mg/L in 5% HNO<sub>3</sub>) from Merck (Darmstadt, Germany) for calibration. AuNP formation was confirmed by means of their shape, size, size distribution, and ζ potential by using different techniques. The hydrodynamic diameter (*d<sub>H</sub>*) and ζ potential of AuNPs were determined by dynamic light scattering (DLS) and electrophoretic light scattering (ELS) methods, respectively, by using the Zetasizer Nano ZS instrument (Malvern Instruments, Malvern, UK) equipped with a green laser (532 nm). Data were processed by the Zetasizer software 6.32 (Malvern Instruments, Malvern, UK). The *d<sub>H</sub>* values were obtained as an average of six replicated measurements and expressed as intensity-weighted size distribution, while the ζ potential was calculated by using the Henry equation with the Smoluchowski approximation from mean values obtained from three replicated ELS measurements. The shape and primary size (*d*) of AuNPs were obtained by using a transmission electron microscope (TEM, 902A; Carl Zeiss Meditec AG, Jena, Germany). The microscope was operated in the bright-field mode at an acceleration voltage of 80 kV. To prepare the sample for TEM imaging, one drop of different AuNP suspensions was deposited on a Formvar-coated copper grid (SPI Supplies, West Chester, PA) and left to air-dry at room temperature. TEM images were captured by a Canon Power-Shot S50 camera, and the primary size (*d*, nm) of

AuNPs was obtained by evaluating 100 particles per AuNP type by the ImageJ software (LOCI, University of Wisconsin, Madison, WI).

UV–vis absorption spectra of functionalized AuNPs were recorded by using an Agilent Cary 3500 UV–vis spectrophotometer (Melbourne, Australia) in the 200–800 nm wavelength range. Quartz cuvettes with an optical path of 10 mm and temperature of 298 K were employed during the measurements.

All pH measurements were made by using an Orion Star A214 Benchtop pH/ISE meter (Thermo Scientific, Waltham, MA) equipped with a glass electrode and Ag–AgCl reference electrode. The pH meter and electrode were calibrated prior to each experiment using Orion pH buffer solutions (Thermo Scientific) of pH 4.01, 7.01, and 10.01.

**NMR Experiments.** To gain structural information about L-DOPA and dopamine during functionalization of AuNPs, <sup>1</sup>H and <sup>13</sup>C{<sup>1</sup>H} NMR spectroscopy was applied by using a Varian INOVA 400 spectrometer (Varian, Palo Alto, CA) operating at 399.6 and 99.9 MHz, respectively. <sup>1</sup>H NMR spectra were recorded at different time points after mixing the reagents and until AuNP formation finished. The spectra were also recorded after AuNP purification to observe the final structural features of catechols bound to the AuNP surface.

In the case of <sup>13</sup>C{<sup>1</sup>H} NMR spectra, recording of AuNPs functionalized with L-DOPA was challenging due to poor solubility, in contrast to dopamine. Therefore, ring-<sup>13</sup>C<sub>6</sub>-labeled L-DOPA (Cambridge Isotope Laboratories GmbH, Radeberg, Germany) was used. The use of the <sup>13</sup>C-enriched L-DOPA enabled observation of carbon atoms of L-DOPA and its oxidation product.

All spectra were recorded at 25 °C. The chemical shifts were expressed in parts per million (ppm) and are referenced to the residual water signal. The WET and PRESAT pulse sequences, available in OpenVnmrJ software (v2.1revA, Inova Varian, Palo Alto, CA), were used to suppress the solvent signals where appropriate.

All NMR experiments were performed under the same condition as used for AuNPs characterization by TEM, DLS, ELS, and UV–vis spectroscopy and described above.

**Density Functional Theory (DFT) Calculations.** DFT methods were employed to examine the mechanism of catechol interaction with Au<sub>*n*</sub> clusters (*n* = 2, 4, 6). Full conformational analysis of L-DOPA and dopamine was conducted by using PC Model software<sup>19</sup> with MMX parameters. All structures within 25 kJ/mol from the global minimum were used for further optimizations with Au<sub>*n*</sub> clusters. For geometry optimizations, the Minnesota 2006 local functional (M06L) and split basis set LANL2DZ//6-31+G(d,p) were used. Generally, Au atoms were optimized by using LANL2DZ and C, H, N, and O atoms by using a 6-31+G(d,p) basis set. Different assemblies of Au<sub>*n*</sub> clusters placed around catechol molecules were generated by using a modified stochastic method.<sup>20</sup>

All calculations were performed by using Gaussian 16 software.<sup>21</sup> All structures and appropriate computational results were visualized with the GaussView program.<sup>22</sup> Implicit solvation was modeled by using the solvent model density continuum (SMD) model.<sup>23</sup> The solvent relative permittivity of ε = 78.4 (water) was used.

Stationary points were characterized by frequency calculation/vibrational analysis to confirm whether the structure is a minimum (no imaginary frequencies) or a first-order saddle point (one imaginary reference). Intrinsic reaction coordinate (IRC) calculations were conducted to identify the minima of reactant and product connected through the respective transition state.<sup>24,25</sup> Energy barriers were calculated as Gibbs free energy difference between transition-state structure and reactant structure with the lowest energy calculated at 298 K.

**Molecular Dynamics (MD) Simulations.** Classical atomistic MD simulations were performed by using the AMBER17 program package.<sup>26</sup> The simulated systems consisted of an Au (111) flat plate (748 atoms distributed in four layers), one of the ligand molecules (leukodopachrome, dopachrome, and quinoid tautomer of dopachrome), and 2000 water molecules. All components were placed in a rectangular box with dimensions of 32 × 43 × 55 Å<sup>3</sup>, and periodic boundary conditions were implemented. The bottom three layers of Au atoms were restrained to maintain the integrity of the plate, while

the top layer was unrestrained. The structures used for ligand molecules were taken from DFT optimizations (lowest energy conformers). Ligand molecules were initially placed 15 Å above the metal surface. The force field used for the description of the metal was the InterfaceFF<sup>27</sup> which was created and previously used for ligand–metal interaction studies.<sup>28</sup> The ligands were described by using the standard GAFF force field found in Amber software, and the water molecules were described by using the TIP3P model. The particle mesh Ewald method was used for electrostatic energy calculations.

Energy minimization was performed for all systems for 1000 cycles by using the steepest descent algorithm. Then, the systems underwent 100 ps of heating where the temperature was raised from 0 to 298 K by using the Langevin thermostat with a collision frequency of 2 ps<sup>-1</sup>. The equilibration phase was performed for 20 ns in the NPT ensemble by using anisotropic pressure scaling and the Berendsen barostat to maintain 1 atm of pressure. The production run was performed for 50 ns in the NVT ensemble. Throughout all phases, the nonbonded interactions cutoff was set to 10 Å, and SHAKE bond length constraints were applied to hydrogen atoms in water.

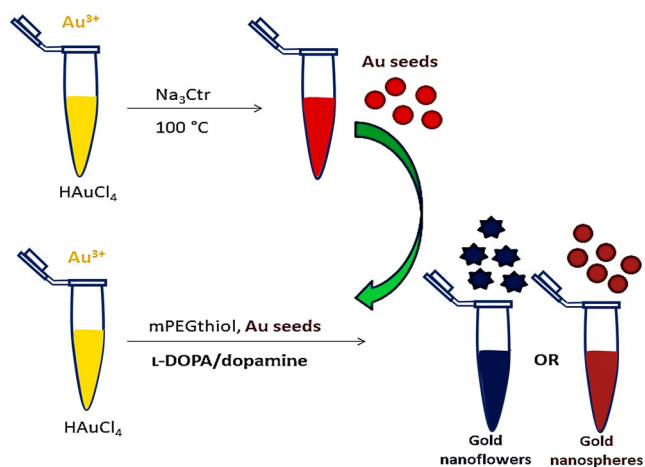
The binding free energy  $\Delta G_{\text{bind}}$  was calculated by using the MM-GBSA protocol available in AmberTools.<sup>26</sup> This method was developed for binding free energy calculations for ligand–receptor systems and previously applied successfully to the interactions of nanomaterials with organic compounds.<sup>29,30</sup> Calculations were based on 1000 trajectory snapshots from the production runs (where the ligands were in contact with the metal).

All images were prepared by using Visual Molecular Dynamics (VMD) software.<sup>31</sup>

## RESULTS AND DISCUSSION

**Formation of AuNPs in the Presence of L-DOPA or Dopamine.** Functionalization of AuNPs was performed by using seed-mediated synthesis (Scheme 1) in which Au seeds were prepared first and used as the growth solution in the mixture of mPEG thiol, HAuCl<sub>4</sub>, and catechol (L-DOPA or dopamine).<sup>13</sup>

**Scheme 1. Schematic Representation of the AuNP Functionalization by the Catechols L-DOPA or Dopamine**



Testing of different experimental conditions revealed that stability, color, and shape of functionalized AuNPs were determined by the molar ratio between Au and catechol (see Table S1 in the Supporting Information). TEM visualization (Figure 1) showed spherical and flowerlike AuNPs. During the bottom-up synthetic approach, the morphology of AuNPs is dictated by the initial aggregation number which is proportional to the amount of reducing agents.<sup>12</sup> When reducing agents are in molar excess, only flower-shaped particles were

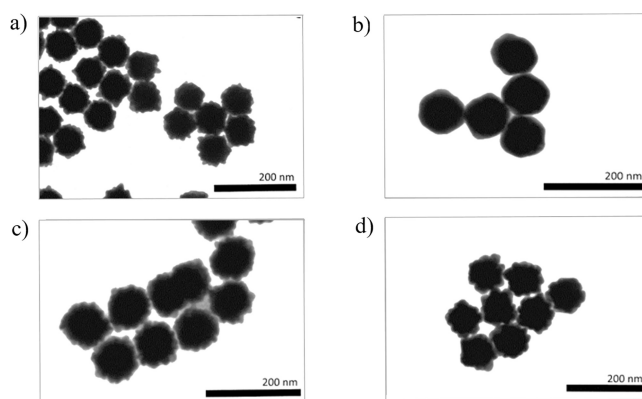


**Figure 1.** TEM micrographs of catechol-functionalized AuNPs obtained at different molar ratio of Au to catechol: (a) [Au]:[dopamine] = 1:6, (b) [Au]:[dopamine] = 2:1, (c) [Au]:[L-DOPA] = 1:6, and (d) [Au]:[L-DOPA] = 2:1.

formed (Figure 1a,c). After initial aggregation of Au seeds, shape directing agents were adsorbed on certain planes of the Au seeds, thus blocking further growth along these sides. Structural defects in the single crystalline species were observed to lower the overall energy of the enlarged particle.<sup>12,32,33</sup> In the case of AuNFs, the twinning motif has changed, inducing migration of newly reduced Au atoms to low energy exposed (111) facets which results in flower-shaped nanostructure.<sup>12,32,33</sup> However, at lower molar ratios of reducing agents, the excess AuCl<sub>4</sub><sup>-</sup> ions will be adsorbed on Au seeds to promote NPs aggregation.<sup>34</sup> Under this condition, spherical AuNPs larger than Au seeds are usually formed.<sup>12,33,35</sup> Contrary to the spherical AuNPs obtained when dopamine was used as reducing agents (Figure 1b), L-DOPA yielded flower-shaped Au nanoparticles (Figure 1d). This difference can be explained by different oxidation processes of L-DOPA and dopamine. Despite using the same molar ratio, L-DOPA oxidation went one step further to dopachrome releasing two additional electrons in comparison to dopamine two-electron oxidation to the quinone form. Hence, L-DOPA has a stronger ability to reduce Au<sup>3+</sup> ions with four electrons, which can in return increase the reaction kinetics. In this way, L-DOPA promotes the rapid deposition process of Au<sup>0</sup> onto the (111) planes, which is key to the formation of multibranching nanocrystals, such as flowerlike nanoparticles.<sup>36</sup>

The primary size (*d*) of all tested AuNPs was below 100 nm, while DLS measurements showed monomodal size distribution with *d<sub>H</sub>* ranging from 97.4 to 119.9 nm (Table S1), irrespective of the catechol type used for functionalization or [Au]:[catechol] ratio. The  $\zeta$  potential ranged from -41.1 to -25.3 mV, with more negative values for molar excess of Au over catechols. The obtained *d*, *d<sub>H</sub>*, and  $\zeta$  potential values for AuNPs obtained at [Au]:[catechol] = 1:6 molar ratio were in accordance with original protocol.<sup>13</sup> Overall, all tested AuNPs showed colloidal stability during our experiments.

UV–vis spectra (Figure S1) showed that all Au nanoflowers were characterized by a surface plasmon resonance (SPR) peak at wavelengths higher than 600 nm, as reported for flowerlike nanoparticles.<sup>13,37</sup> In the case of spherical dopamine-functionalized AuNPs, the SPR peak was at 575 nm as described for spherical AuNPs.<sup>38</sup> A redshift in the SPR peak was observed for AuNPs functionalized with L-DOPA compared to



## Scheme 2. Schematic Representation of Dopamine Oxidation in an Acidic Environment (pH $\approx$ 3)

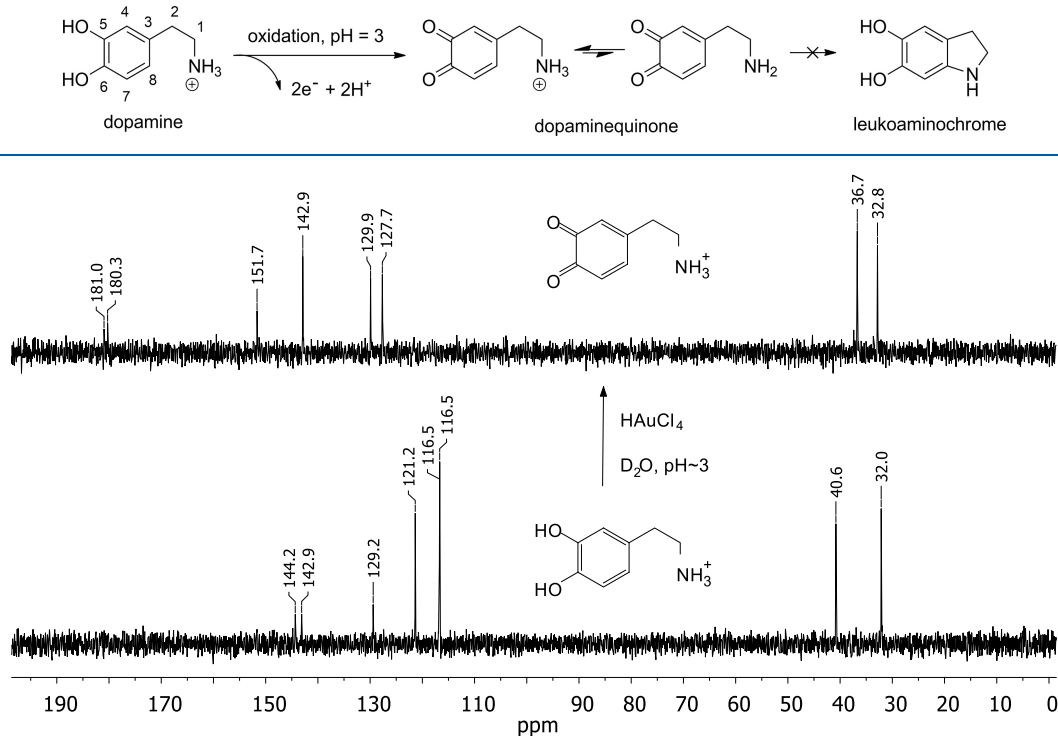


**Figure 2.**  $^{13}\text{C}$  NMR spectra of dopamine (10 mM) and dopamine oxidation product (dopamine quinone) in  $\text{D}_2\text{O}$  (pH  $\approx$  3;  $[\text{Au}]:[\text{dopamine}] = 2:1$ , as used for the preparation of stable spherical AuNPs).

dopamine, which can be explained by the increase in AuNP size as confirmed by TEM and DLS measurements.<sup>39</sup>

In each reaction mixture and each AuNP suspension after purification, the pH ranged between 3.15 and 3.25. Contrary to comprehensive investigations of L-DOPA and dopamine autoxidation in alkaline and neutral conditions,<sup>6,40–45</sup> oxidation processes of these two catechols in an acidic environment have not been thoroughly described. As transition-metal ions can promote their oxidation in mildly acidic pH, this has attracted interest.<sup>46</sup> Therefore, the interactions of dopamine or L-DOPA with  $\text{Au}^{3+}$  ions, Au nanoclusters, Au seeds, or AuNPs, each present at different time points of the AuNP functionalization process, were investigated as this occurred in an acidic environment.

**NMR Study of AuNPs Interaction with Dopamine.** In the acidic aqueous medium, dopamine is stable for days. No oxidation or degradation products were observed in  $^1\text{H}$  or  $^{13}\text{C}$  NMR spectra of 10 mM dopamine in deuterated water (pD = 3). In an alkaline medium, however, dopamine undergoes oxidation followed by different transformation and polymerization processes.<sup>46,47</sup> In the  $^1\text{H}$  NMR spectrum of 10 mM dopamine in deuterated water (pD = 10, NaOD added), all aromatic signals disappeared after ca. 3 h, and a series of broadened signals in the upfield region appeared (Figure S2). This suggests the formation of a mixture of melanin oligomers, for example, eumelanin, pheomelanin, or dihydroxyindole melanin (Scheme S1).

Dopamine may be easily oxidized in an acidic medium in the presence of  $\text{HAuCl}_4$ . We report herewith that the extent of the oxidation reaction depended on the molar ratio of reactants  $\text{HAuCl}_4$  and dopamine, that is, the  $[\text{Au}]:[\text{dopamine}]$  ratio, which also determined the shape, stability, and color of AuNPs (Table S1 and Figure 1). In the case of excess Au, that is,  $[\text{Au}]$ :

$[\text{dopamine}] = 2:1$ ; as used for the preparation of stable spherical AuNPs, Figure 1), dopamine was rapidly and completely oxidized to dopamine quinone (Scheme 2 and Figure S3a), which remained stable for >2 h.

On the contrary, when dopamine was in large excess, that is,  $[\text{Au}]:[\text{dopamine}] = 1:6$ , no dopamine oxidation product was observed during the preparation of stable Au nanoflowers. NMR signals for dopamine remained unchanged after 2 h (Figure S3c). If two reactants were equimolar, the equivalent amount of dopamine and dopamine quinone was formed in the reaction (Figure S3b).

The mixture of products formed during the preparation of AuNPs may be governed by the  $[\text{Au}]:[\text{dopamine}]$  ratio; that is, the type of coating on AuNP surfaces appears to depend on the initial reaction conditions. This is supported by  $^1\text{H}$  NMR spectra of isolated and purified AuNPs (Figure S4). If the initial ratio of reactants was  $[\text{Au}]:[\text{dopamine}] = 1:6$ , the prepared AuNPs were coated with dopamine only (Figure S4b). In the case when Au was in excess, the surface of the prepared AuNPs was modified with dopamine quinone (Figure S4c). In both cases, proton signals in the upfield region of the  $^1\text{H}$  NMR spectrum were broadened and less resolved, while no broadening was observed in the aromatic region. This indicates that only the alkylamino moiety of dopamine/dopamine quinone was involved in the interaction with the AuNP surface.

The structure of dopamine quinone was confirmed by  $^1\text{H}$  and  $^{13}\text{C}$  NMR spectra, with the latter reported for the first time (Figure 2). In the  $^1\text{H}$  spectrum (Figure S3a), three new signals appeared in the aromatic region and two new signals in the upfield region (Table 1). In the  $^{13}\text{C}$  spectrum, all aromatic signals were shifted downfield, with two carbonyl signals characterized by the largest chemical shifts (180.96 and 180.27

**Table 1. <sup>1</sup>H and <sup>13</sup>C NMR Data for Dopamine and Dopamine Quinone in Acidic Aqueous Medium (pH = 3)**

NMR expt	dopamine		dopamine quinone		assign <sup>a</sup>
	$\delta$ (ppm)	$J(\text{H, H})$ (Hz)	$\delta$ (ppm)	$J(\text{H, H})$ (Hz)	
<sup>1</sup> H NMR	6.75	d (8.1)	7.00	dd (10.2, 2.1)	H4
	6.69	d (2.1)	6.34	d (10.2)	H8
	6.60	dd (8.1, 2.1)	6.23	d (2.1)	H7
	3.07	t (7.3)	3.17	t (7.5)	H1
	2.72	t (7.3)	2.70	t (7.5)	H2
<sup>13</sup> C NMR	144.16	s	180.96	s	C5/C6
	142.93	s	180.27	s	C5/C6
	129.23	s	151.65	s	C3
	121.18	d	142.89	d	C8
	116.53	d	129.91	d	C4/C7
	116.49	d	127.66	d	C4/C7
	40.63	t	36.71	t	C1
	31.95	t	32.84	t	C2

<sup>a</sup>As denoted in Scheme 2.

ppm). This is consistent with the structure of dopamine quinone obtained during AuNP formation and is in line with the earlier structural assignments of dopamine oxidation products.<sup>40</sup> No proton signals corresponding to leukoaminochrome, aminochrome, and/or 5,6-dihydroxyindole were observed, which confirmed that cyclization of dopamine quinone did not occur.

It is known that cyclization of dopamine quinone may be induced by the increased pH value,<sup>46,48,49</sup> by the increased voltage in the electrochemical oxidation,<sup>50</sup> via a hydrothermal method,<sup>51</sup> or by using plasma-activated water.<sup>52</sup> None of these reaction procedures, however, are relevant for the original protocol<sup>13</sup> used here for AuNP functionalization with dopamine.

To summarize, the extent of the oxidation of dopamine with H<sub>2</sub>AuCl<sub>4</sub> is controlled by the molar ratio of reactants (H<sub>2</sub>AuCl<sub>4</sub> and dopamine). In no case was the formation of dopamine quinone, the main oxidation product, followed by intra-

molecular cyclization. Thus, purified AuNPs may be coated by dopamine itself, dopamine quinone, or a mixture of both.

**NMR Study of AuNPs Interaction with L-DOPA.** Similar to dopamine, L-DOPA is stable in the acidic aqueous medium. No change in <sup>1</sup>H or <sup>13</sup>C NMR spectra of 10 mM L-DOPA in D<sub>2</sub>O (pD = 3) was observed for days. As expected, in the alkaline aqueous medium (pD = 11, NaOD added) all proton signals of L-DOPA disappeared within 1 h, and a series of new signals in the upfield region of the <sup>1</sup>H spectrum emerged (Figure S5). According to the literature, different forms of melanin oligomers or polydopa may be associated with the observed spectrum of the mixture.<sup>6,53</sup>

The oxidation of L-DOPA in an acidic environment may be catalyzed by H<sub>2</sub>AuCl<sub>4</sub> if the latter is used in excess. The ratio of [Au]:[L-DOPA] = 2:1, which corresponds to the protocol for the preparation of stable Au nanoflowers, was employed. Immediately after mixing of reactants, all proton signals of L-DOPA disappeared from the <sup>1</sup>H NMR spectrum, and three new signals appeared (green spectrum in Figure S6). The new set of signals in the aromatic and upfield regions correspond to dopaquinone (Table 2). To our knowledge, this is the first NMR evidence of the initial oxidation product of L-DOPA. Because of the short lifetime of dopaquinone (see below), the well-resolved <sup>13</sup>C NMR spectrum was difficult to record. For this reason, the reaction was repeated by using ring-<sup>13</sup>C<sub>6</sub>-labeled L-DOPA, which enabled facile and fast observation of all carbon signals (Figure 3) in the aromatic region.

The dopaquinone is not stable but undergoes intramolecular cyclization in which leukodopachrome/dopachrome is formed (Scheme 3). In contrast to dopamine quinone (see above), the intramolecular cyclization or Michael addition reaction occurs easily in dopaquinone. In the <sup>1</sup>H NMR spectrum (Table 2 and Figure S6, blue spectrum) two new signals appeared in the aromatic region which correspond to leukodopachrome or its oxidized counterpart dopachrome. It is known that leukodopachrome is more easily oxidized than L-DOPA itself.<sup>54</sup> Both leukodopachrome and its oxidized form dopachrome may exist in a fast redox equilibrium, which is difficult to resolve on the NMR time scale. In addition, dopachrome may tautomerize to its isomeric quinoid structure. The latter is expected to display

**Table 2. <sup>1</sup>H and <sup>13</sup>C NMR Data for L-DOPA and Its Oxidized Products Dopaquinone and Dopachrome in Acidic Aqueous Medium (pH = 3)**

NMR expt	L-DOPA		dopaquinone		dopachrome		assign <sup>a</sup>
	$\delta$ (ppm)	$J(\text{H, H})$ (Hz)	$\delta$ (ppm)	$J(\text{H, H})$ (Hz)	$\delta$ (ppm)	$J(\text{H, H})$ (Hz)	
<sup>1</sup> H NMR	6.74	d (8.3)	7.02	dd (10.2, 1.8)	6.99	t (0.9)	H4
	6.66	d (1.2)	6.35	d (10.3)			H8
	6.58	dd (8.3, 1.2)	6.29	d (1.8)	6.57	s	H7
	3.78	dd (7.9, 5.9)	4.27	t (7.1)	4.15	t (7.0)	H1
	3.00	dd (5.9, 14.7)	3.02	dd (6.7, 15.0)	2.98	dd (7.0, 14.4)	H2
	2.84	dd (7.9, 14.7)	2.89	dd (7.6, 14.8)	2.86	dd (7.2, 14.0)	H2
<sup>13</sup> C NMR	173.91	s					
	143.78	m	187.1	m	180.9	m	C5/C6
	143.76	m	181.9	m	180.2	m	C5/C6
	127.57	m	155.8	m	149.5	m	C3
	121.78	m	143.6	m	142.4	m	C8
	116.72	m	133.2	m	130.6	m	C4/C7
	116.68	m	132.7	m	129.4	m	C4/C7
	56.00	s					C1
	35.50	d (45.0)					C2

<sup>a</sup>As denoted in Scheme 3.

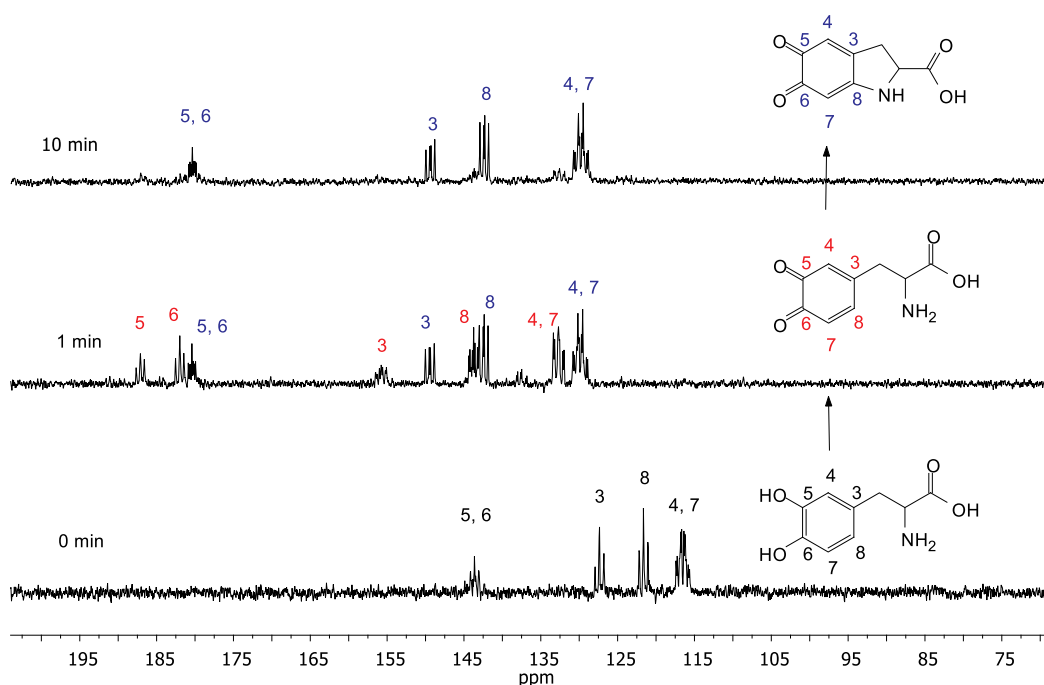
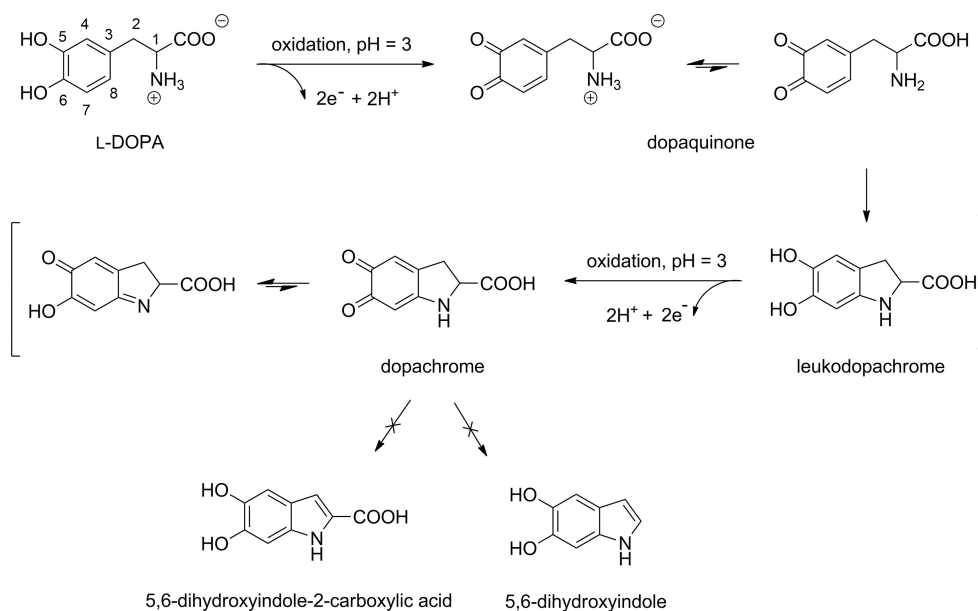


**Figure 3.**  $^{13}\text{C}$  NMR spectra of L-DOPA (bottom spectrum, black numbers), its oxidation intermediates dopaquinone/dopachrome (middle spectrum, red/blue numbers), and dopachrome (top spectrum, blue numbers) in  $\text{D}_2\text{O}$  ( $\text{pH} \approx 3$ ;  $[\text{Au}]:[\text{L-DOPA}] = 2:1$ , as used for the preparation of stable Au nanoflowers). All ring carbon atoms 3–8 are  $^{13}\text{C}$ -enriched.

**Scheme 3. Schematic Representation of L-DOPA Oxidation in an Acidic Environment ( $\text{pH} \approx 3$ )<sup>a</sup>**



<sup>a</sup>Structures in square brackets cannot be differentiated by  $^1\text{H}$  NMR spectroscopy (in  $\text{D}_2\text{O}$ ). All structures may exist in zwitterion form.

a pattern of signals in the  $^1\text{H}$  NMR spectrum, which is very similar to that of leukodopachrome and/or dopachrome. A similar spectral ambiguity applies to the  $^{13}\text{C}$  NMR spectrum.

Dopaquinone is less stable than leukodopachrome and/or dopachrome under the experimental conditions used. According to our calculations (see below), the structure of leukodopachrome is 85 kJ/mol more stable than dopaquinone. In the  $^1\text{H}$  NMR spectrum, all signals of dopaquinone disappeared in 10 min, whereas the latter intermediates (leukodopachrome/dopachrome) persisted in the reaction mixture for ca. 2 h. This means that the subsequent

rearrangement of dopachrome to 5,6-dihydroxyindole-2-carboxylic acid or decarboxylation to 5,6-dihydroxyindole are slower processes than the cyclization of dopaquinone. Neither 5,6-dihydroxyindole-2-carboxylic acid nor 5,6-dihydroxyindole structures matches the experimental chemical shifts observed in the  $^1\text{H}$  and/or  $^{13}\text{C}$  NMR spectra. The most conclusive evidence comes from the  $^{13}\text{C}$  NMR spectrum in which two  $\text{sp}^3$ -hybridized carbon signals are detected in the upfield region, which eliminates 5,6-dihydroxyindole-2-carboxylic acid and 5,6-dihydroxyindole as possible oxidation products.

In short, at least three different oxidation products of L-DOPA may be included in interactions with the AuNP surface: leukodopachrome, dopachrome, or its tautomeric form (structures in square brackets in Scheme 3). These three intermediates cannot be differentiated by  $^1\text{H}$  NMR spectroscopy. L-DOPA itself may bind with the nanosurface during the preparation of AuNPs if the synthesis is performed with a large excess of L-DOPA ( $[\text{Au}]:[\text{L-DOPA}] = 1:6$ ; as used for the preparation of stable Au nanoflowers). This is confirmed by the  $^1\text{H}$  NMR spectrum recorded after purification (Figure S7b). Only dopaquinone is a poor candidate for AuNP coating as it undergoes fast cyclization under the reaction conditions employed.

**DFT Calculations.** To rationalize the mechanism underlying the oxidation processes in catechols during AuNP synthesis and functionalization, DFT calculations were performed. Of particular importance is the analysis of the different reactivity of dopaquinone and dopamine quinone in terms of their intramolecular cyclization.

During the initial oxidation, both L-DOPA and dopamine are converted to corresponding quinones, which may undergo intramolecular Michael addition (Schemes 2 and 3). In this reaction, the amino group with lone-pair electrons attacks the C5 position in the oxidized catechol ring. According to the literature, experimental barriers (at 298 K) for the intramolecular cyclization of dopaquinone ( $\Delta G^\ddagger = 62.3$  kJ/mol) and dopamine quinone ( $\Delta G^\ddagger = 64.8$  kJ/mol) are very similar.<sup>55,56</sup>

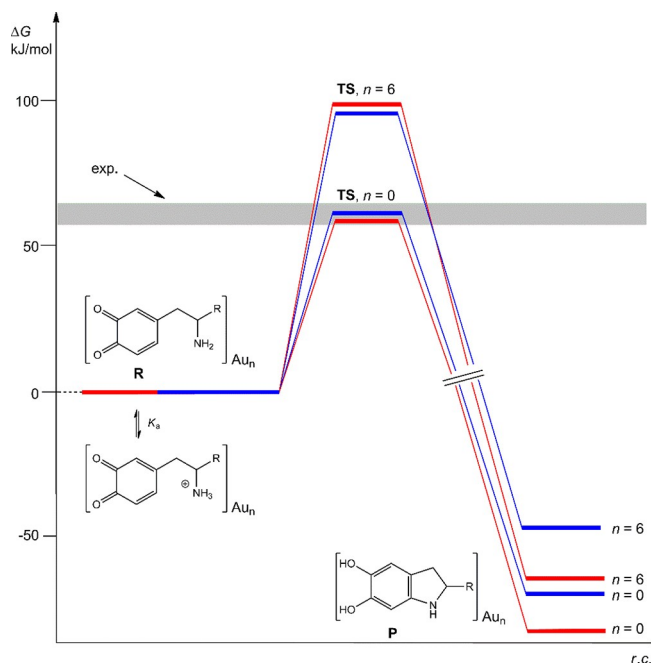
These experimental data are reproduced at the SMD-M06L/6-31+G(d,p)/LANL2DZ level of theory ( $\Delta G^\ddagger = 63.3$  and 58.9 kJ/mol, respectively; see Scheme 4), which confirms that intrinsic cyclization rates are comparable and relatively rapid in both cases. The rate-determining step of cyclization involves the unprotonated form of the amino group, and therefore the reaction rate is strongly pH dependent. In our case, in the presence of  $\text{HAuCl}_4$  at a relatively low pH, the cyclization was observed only in the case of dopaquinone (see above).

This different reactivity of dopaquinone and dopamine quinone has been related to a fraction of the neutral amino group, as defined by preequilibrium acidity constant  $K_a$  (Scheme 4). It is known that the  $\text{p}K_a$  value ( $\text{NH}_3^+$ ) value in dopaquinone is ca. 2 units lower than in dopamine quinone, producing a 10-fold difference in the cyclization rates.<sup>46,49</sup>

To assess the effect of AuNPs on the cyclization rate, the reactants dopaquinone and dopamine quinone, transition states, and products (leukodopachrome and leukoaminochrome) were modeled as structures complexed to the neutral cluster  $\text{Au}_n$ , where  $n = 2, 4$ , or 6 (see Figure 4). In comparison to the metal-free reaction ( $n = 0$ ), the calculated barriers ( $\Delta G^\ddagger$ ) for all  $\text{Au}_n$ -assisted cyclizations were increased by 30–40 kJ/mol (Scheme 4 and Table 3). Again, the estimated rates for the intramolecular Michael *N*-additions were similar for dopaquinone and dopamine quinone. The calculated range of energy barriers ( $\Delta G^\ddagger = 91.7$ – $101.9$  kJ/mol), using the Eyring equation that results from transition state theory, corresponds to reaction rate constants  $k_{\text{obs}} \approx 5 \times 10^{-4}$ – $9 \times 10^{-6} \text{ s}^{-1}$  ( $t_{1/2} \approx 0.4$ – $20.8 \text{ h}^{-1}$ ).

The influence of  $\text{Au}_n$  clusters on the  $\text{p}K_a$  value of the ionizable amino group may be negligible.<sup>46</sup> Therefore, different rates for cyclization of dopaquinone and dopamine quinone, as observed experimentally, are not induced by  $\text{Au}_n$  nanoclusters. In contrast to dopamine quinone, the dopaquinone easily

**Scheme 4. Gibbs Free Energy Diagram for Intramolecular Cyclization of Dopamine Quinone (R = H; Blue Line) and Dopaquinone (R = COOH; Red Line) Calculated at the SMD-M06L/6-31+G(d,p)/LANL2DZ Level (Solvent = Water)<sup>a</sup>**



<sup>a</sup>All stationary points (R, TS, and P) are complexed to a specified number of Au atoms ( $n = 0, 2, 4$ , or 6). The gray band denotes the experimental barrier for the Au-free process ( $n = 0$ ) in dopaquinone and dopamine quinone. TS structures are presented in Figures 4 and S8.

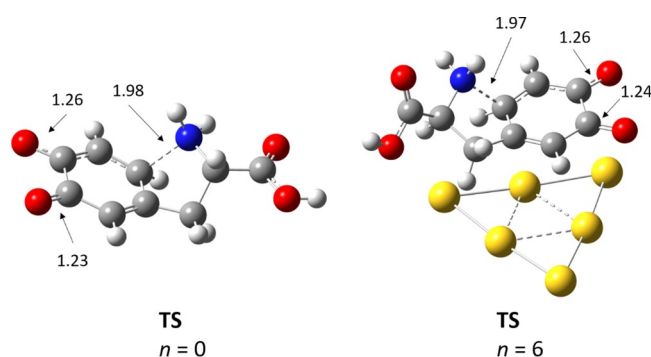


**Figure 4.** SMD-M06L/6-31+G(d,p)/LANL2DZ (solvent = water) optimized transition state structures for the intramolecular cyclization of dopaquinone in the presence of  $\text{Au}_n$  cluster ( $n = 6$ , right) and in a metal-free process ( $n = 0$ , left). All distances are in Å.

undergoes intramolecular cyclization, which is related to its (larger) intrinsic acidity of the nucleophilic amino group.

According to our calculated results, the formation of cyclized products is strongly exergonic; that is, the leukodopachrome and leukoaminochrome are more stable than the starting dopaquinone and dopamine quinone, respectively. In the case of metal-free and Au-assisted reactions, cyclized products were 25–75 kJ/mol stable (Table 3), which means that both reactions are thermodynamically favored. The estimated barriers for Au-assisted reactions ( $\Delta G^\ddagger \approx 100$  kJ/mol) suggest that both reactions may be kinetically feasible. However, because of the more protonated ionization state ( $\text{NH}_3^+$ ) in



**Table 3. SMD-M06L/6-31+G(d,p)/LANL2DZ Calculated Relative Energies ( $\Delta G_{298}$  in kJ/mol) of Stationary Points Involved in the Intramolecular Cyclization of Dopamine Quinone and Dopamine Quinone, Where R Is a Reactant, TS Is a Transition State, and P Is a Product (Leukodopachrome and Leukoaminochrome, Respectively), Complexed to a Number of Au Atoms Specified by  $n$**

$Au_n$	stationary point	$\Delta G_{298}$ (kJ/mol)	
		dopaquinone	dopamine quinone
$n = 0$	R	0.0	0.0
	TS	+63.3	+58.9
	P	-85.0	-74.1
$n = 2$	R	0.0	0.0
	TS	+94.1	+97.5
	P	-38.9	-26.4
$n = 4$	R	0.0	0.0
	TS	+101.9	+101.7
	P	-17.7	-25.9
$n = 6$	R	0.0	0.0
	TS	+91.6	+97.1
	P	-63.8	-47.2

dopamine quinone, the latter does not undergo the nucleophilic Michael N-addition. Under our reaction conditions, the cyclized product was observed only in the case of dopaquinone.

The formation of leukodopachrome may be followed by its oxidation to dopachrome, which exists in equilibria with its quinoid tautomer (Scheme 3). The definitive form of intermediate, which accumulates in the presence of the  $Au_n$  clusters, is not easily discernible (see NMR data). To assess which oxidation product may occur as a candidate for AuNP coating, classical MD simulations were performed. These calculations provide binding free energies (see below), which provided an estimate on the interaction/stability of different species at the AuNP surface.

**Adsorption of L-DOPA Oxidation Intermediates on Au Nanosurface—Atomistic Molecular Dynamics Simulations.** To compare the adsorption of L-DOPA oxidation intermediates (leukodopachrome, dopachrome, and its quinoid tautomer) on the AuNPs, we performed atomistic molecular dynamics (MD) simulations of the three molecules in the presence of an Au nanosurface (Figure 5). This model simulated the adsorption through physical interactions as classical MD does not allow covalent bond formation.<sup>57</sup> In all cases, the species descend from their initial positions and bind to the Au surface within the first 10 ns of the corresponding unrestrained MD simulations, where they persist for the entire duration of the *in silico* experiments (50 ns). By computing the

vertical component ( $z$ -axis) of the distance  $d_z$  between the Au nanosurface and each heteroatom of the studied ligands, we could confirm that all functional groups are involved in the interaction between the oxidized species and the Au surface ( $d_z < 6$  Å for the whole simulation time frame), as shown in Figures 6A–C and S9. The analysis of the mean-square displacement (MSD) along the three spatial directions reveals a similar behavior for all the oxidized species, as illustrated in Figure 6D for dopachrome as an example. In particular, the molecular displacements among the  $z$ -component are found to be consistently low for the three molecules, thereby confirming the observation that each Au/ligand binding is sufficiently weak to allow for ligand lateral diffusion but strong enough to prevent its desorption (Figure 6E and Movies S1–S3). Of note, our results are in line with previous findings from similar studies.<sup>18,58–60</sup>

The adsorption free energy of each ligand onto the Au nanosurface was next calculated via the MM-GBSA method. While this computational procedure is not fully reliable in calculating absolute energies, it has been established to be accurate enough in assessing relative binding energies and is thus widely adopted in comparing/ranking the affinities of similar ligands for a given receptor.<sup>56</sup> In aggregate, the MM-GBSA results at room temperature indicate that the all three molecular adsorption processes are exergonic (i.e., thermodynamically spontaneous); moreover, according to the calculations, dopachrome is endowed with the highest affinity for the Au nanosurface ( $\Delta G_{\text{bind}} = -182.9$  kJ/mol) followed by, in the order, leukodopachrome ( $\Delta G_{\text{bind}} = -160.9$  kJ/mol) and the dopachrome tautomer ( $\Delta G_{\text{bind}} = -125.0$  kJ/mol). This helped to determine which oxidation intermediate is the best candidate for AuNP functionalization. In our case, MD simulation results coupled with NMR analysis (see above) confirmed that the surface of prepared AuNPs is modified only with dopachrome.

## CONCLUSION

This study focused on the transformation patterns of L-DOPA and dopamine during their interaction with  $Au^{3+}$  ions, Au nanoclusters, and the AuNP surface. A combination of spectroscopy, light scattering, and microscopy techniques was used, while structural information and reaction mechanism were obtained by NMR experiments combined with computation tools.

Experimental results revealed that the extent of catechol oxidation correlated to their molar ratio to Au used for AuNP preparation and were supported by computational methods. To prepare AuNPs functionalized with fully reduced catechols, a large molar excess of L-DOPA or dopamine is needed. In the case of molar excess of Au, the oxidation of catechols to

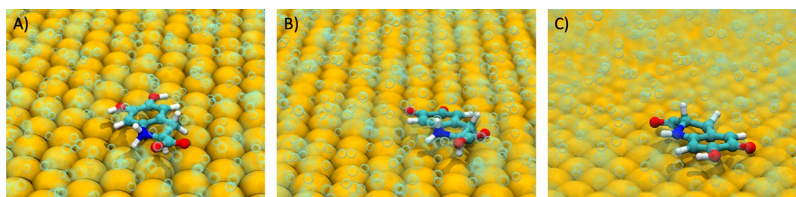


**Figure 5.** Close-up snapshots of the last frames of the production runs from classical atomistic MD simulations of the zwitterionic forms of (A) leukodopachrome, (B) dopachrome, and (C) dopachrome tautomer on the Au(111) surface. Au atoms (dark yellow) are represented via their van der Waals spheres; the three ligand molecules are shown in a balls-and-sticks representation (color code: cyan, C; red, O; blue, N; white, H), and the oxygen atoms of the water molecules are portrayed as semitransparent cyan spheres.



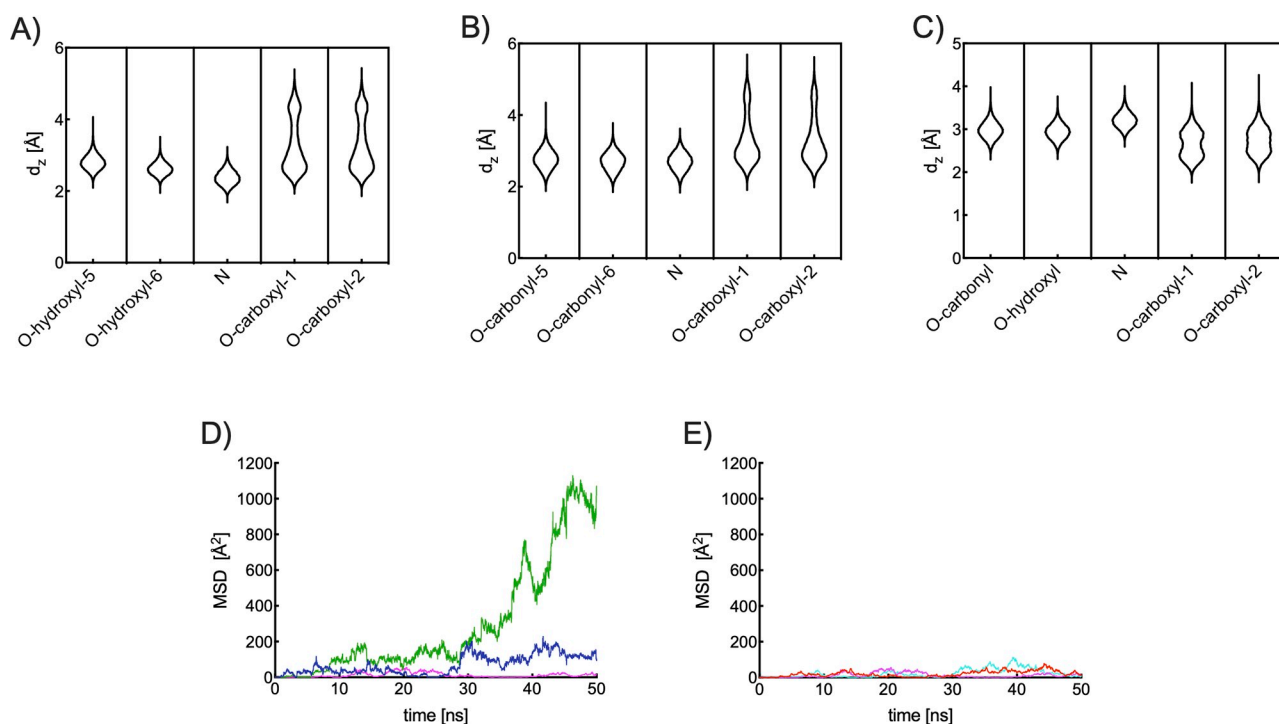


**Figure 6.** Violin plots of the distance  $d_z$  along the vertical component between the Au nanosurface and each heteroatom for leukodopachrome (A), dopachrome (B), and dopachrome tautomer (C). (D) Mean-square displacement (MSD) of dopachrome on the Au nanosurface computed along the three spatial directions ( $x$ , green;  $y$ , blue;  $z$ , magenta) during the relevant MD production run. (E) Comparison of the MSDs computed along the vertical ( $z$ ) direction for leukodopachrome (cyan), dopachrome (magenta), and dopachrome tautomer (red) during the corresponding MD simulation production runs.

dopamine quinone and dopaquinone was promoted. In contrast to dopamine quinone, the latter underwent intramolecular cyclization in which additional oxidation products, leukodopachrome, dopachrome, or its tautomer, were formed. These oxidation products may be considered as possible forms attached to the AuNP surface when synthesis is performed in an excess of Au. To differentiate these three species, the combination of NMR spectroscopy and computational methods is warranted. DFT results showed that different rates for cyclization of dopaquinone and dopamine quinone were not induced by Au<sub>n</sub> nanoclusters but by the larger intrinsic acidity of the more nucleophilic amino group in dopaquinone. Formation of cyclized products is strongly exergonic, while metal-free and Au-assisted reaction are both thermodynamically favored and kinetically feasible. MD simulations clarified the most likely candidates, among different oxidation products, for binding to the AuNP surface. The highest affinity was obtained for dopachrome compared to its tautomer and leukodopachrome.

The methodological approach presented here led to the reliable characterization of molecules bound at the nanosurface resulting from a functionalization strategy of AuNPs with L-DOPA and dopamine.

## ■ ASSOCIATED CONTENT

### SI Supporting Information

The Supporting Information is available free of charge at <https://pubs.acs.org/doi/10.1021/acs.inorgchem.2c00996>.

Additional information about AuNPs preparation and characterization (optimization of AuNPs synthesis and AuNPs characterization by UV-vis spectroscopy); additional NMR results; supplemental computational

information; references; XYZ coordinates of all structures from theoretical calculations (PDF)

Movie S1 (MP4)

Movie S2 (MP4)

Movie S3 (MP4)

## ■ AUTHOR INFORMATION

### Corresponding Author

Ivana Vinković Vrček – Institute for Medical Research and Occupational Health, 10000 Zagreb, Croatia; [orcid.org/0000-0003-1382-5581](https://orcid.org/0000-0003-1382-5581); Phone: +38514682540; Email: [ivinkovic@imi.hr](mailto:ivinkovic@imi.hr)

### Authors

Nikolina Kalčec – Institute for Medical Research and Occupational Health, 10000 Zagreb, Croatia

Antonio Ljulj – Faculty of Pharmacy and Biochemistry, University of Zagreb, 10000 Zagreb, Croatia

Lucija Božičević – Institute for Medical Research and Occupational Health, 10000 Zagreb, Croatia; [orcid.org/0000-0001-5222-7678](https://orcid.org/0000-0001-5222-7678)

Valerije Vrček – Faculty of Pharmacy and Biochemistry, University of Zagreb, 10000 Zagreb, Croatia; [orcid.org/0000-0003-1624-8126](https://orcid.org/0000-0003-1624-8126)

Domenico Marson – Molecular Biology and Nanotechnology Laboratory (MolBNL@UniTS), DEA, University of Trieste, 34127 Trieste, Italy

Sabrina Pricl – Molecular Biology and Nanotechnology Laboratory (MolBNL@UniTS), DEA, University of Trieste, 34127 Trieste, Italy; Department of General Biophysics, University of Łódź, 90-236 Łódź, Poland

Frances Separovic – School of Chemistry, Bio21 Institute,  
University of Melbourne, Melbourne, VIC 3010, Australia;  
orcid.org/0000-0002-6484-2763

Complete contact information is available at:  
<https://pubs.acs.org/10.1021/acs.inorgchem.2c00996>

## Funding

This study was financially supported by the “Research Cooperability” Program of the Croatian Science Foundation funded by the European Union from the European Social Fund under the Operational Programme Efficient Human Resources 2014–2020 (Grant HRZZ-PZS-2019-02-4323).

## Notes

The authors declare no competing financial interest.

## ACKNOWLEDGMENTS

This publication is based upon work from COST Action CA 17140 “Cancer Nanomedicine from the Bench to the Bedside” supported by the COST (European Cooperation in Science and Technology). We thank Barbara Pem, PhD, for preliminary work with MD simulations. We acknowledge the use of Isabella cluster based in the University Computing Centre SRCE, University of Zagreb,<sup>62</sup> and computer cluster [sw.pharma.hr](http://sw.pharma.hr), acquired through the ESF-ERDF financed FarmInova project #KK.01.1.1.02.0021 and based in the Faculty of Pharmacy and Biochemistry.

## REFERENCES

- (1) Chowdhury, A.; Kunjiappan, S.; Panneerselvam, T.; Somasundaram, B.; Bhattacharjee, C. Nanotechnology and Nano-carrier-Based Approaches on Treatment of Degenerative Diseases. *Int. Nano Lett.* **2017**, *7*, 91–122.
- (2) Baptista, P.; Fernandes, A.; Figueiredo, S.; Vinhas, R.; Cordeiro, M.; Carlos, F.; Mendo, S. Gold Nanoparticle-Based Theranostics: Disease Diagnostics and Treatment Using a Single Nanomaterial. *Nanobiosensors Dis. Diagnosis* **2015**, *4*, 11–23.
- (3) Liu, X.; He, F.; Zhang, F.; Zhang, Z.; Huang, Z.; Liu, J. Dopamine and Melamine Binding to Gold Nanoparticles Dominates Their Aptamer-Based Label-Free Colorimetric Sensing. *Anal. Chem.* **2020**, *92*, 9370–9378.
- (4) Zhang, Y.; Li, B.; Chen, X. Simple and Sensitive Detection of Dopamine in the Presence of High Concentration of Ascorbic Acid Using Gold Nanoparticles as Colorimetric Probes. *Microchim. Acta* **2010**, *168*, 107–113.
- (5) Sun, J.; Jiang, S.; Xu, J.; Li, Z.; Li, C.; Jing, Y.; Zhao, X.; Pan, J.; Zhang, C.; Man, B. Sensitive and Selective Surface Plasmon Resonance Sensor Employing a Gold-Supported Graphene Composite Film/D-Shaped Fiber for Dopamine Detection. *J. Phys. D: Appl. Phys.* **2019**, *52*, 195402.
- (6) Hormozi-Nezhad, M. R.; Moslehipour, A.; Bigdeli, A. Simple and Rapid Detection of L-Dopa Based on in Situ Formation of Polylevodopa Nanoparticles. *Sensors Actuators, B Chem.* **2017**, *243*, 715–720.
- (7) Lu, C. C.; Zhang, M.; Li, A. J.; He, X. W.; Yin, X. B. 3,4-Dihydroxy-L-Phenylalanine for Preparation of Gold Nanoparticles and as Electron Transfer Promoter in H<sub>2</sub>O<sub>2</sub> Biosensor. *Electroanalysis* **2011**, *23*, 2421–2428.
- (8) Rostami, A.; Hadjizadeh, A.; Mahshid, S. Colorimetric Determination of Dopamine Using an Electrospun Nanofibrous Membrane Decorated with Gold Nanoparticles. *J. Mater. Sci.* **2020**, *55*, 7969–7980.
- (9) Mohseni, N.; Bahram, M. Highly Selective and Sensitive Determination of Dopamine in Biological Samples via Tuning the Particle Size of Label-Free Gold Nanoparticles. *Spectrochim. Acta - Part A Mol. Biomol. Spectrosc.* **2018**, *193*, 451–457.
- (10) Hu, K.; Chen, X.; Chen, W.; Zhang, L.; Li, J.; Ye, J.; Zhang, Y.; Zhang, L.; Li, C. H.; Yin, L.; Guan, Y. Q. Neuroprotective Effect of Gold Nanoparticles Composites in Parkinson’s Disease Model. *Nanomedicine Nanotechnology, Biol. Med.* **2018**, *14*, 1123–1136.
- (11) Sim, T. M.; Tarini, D.; Dheen, S. T.; Bay, B. H.; Srinivasan, D. K. Nanoparticle-Based Technology Approaches to the Management of Neurological Disorders. *Int. J. Mol. Sci.* **2020**, *21*, 1–32.
- (12) Sajitha, M.; Vindhyasarumi, A.; Gopi, A.; Yoosaf, K. Shape Controlled Synthesis of Multi-Branched Gold Nanocrystals through a Facile One-Pot Bifunctional Biomolecular Approach. *RSC Adv.* **2015**, *5*, 98318–98324.
- (13) Ong, Z. Y.; Chen, S.; Nabavi, E.; Regoutz, A.; Payne, D. J.; Elson, D. S.; Dexter, D. T.; Dunlop, I. E.; Porter, A. E. Multibranching Gold Nanoparticles with Intrinsic LAT-1 Targeting Capabilities for Selective Photothermal Therapy of Breast Cancer. *ACS Appl. Mater. Interfaces* **2017**, *9*, 39259–39270.
- (14) Gonzalez-Carter, D. A.; Ong, Z. Y.; McGilvery, C. M.; Dunlop, I. E.; Dexter, D. T.; Porter, A. E. L-DOPA Functionalized, Multi-Branched Gold Nanoparticles as Brain-Targeted Nano-Vehicles. *Nanomedicine Nanotechnology, Biol. Med.* **2019**, *15*, 1–11.
- (15) Qu, W. G.; Wang, S. M.; Hu, Z. J.; Cheang, T. Y.; Xing, Z. H.; Zhang, X. J.; Xu, A. W. In Situ Synthesis of Gold@3,4-Dihydroxy-L-Phenylalanine Core-Shell Nanospheres Used for Cell Imaging. *J. Phys. Chem. C* **2010**, *114*, 13010–13016.
- (16) Li, G.; Yang, M.; Chen, L. C.; Gao, B.; Xiong, X. L. Colorimetric and Visual Detection of Tyrosine Based on Its Copper-Catalyzed Enzymatic Oxidation to Dopamine and Subsequent Reductive Formation of Colored Gold Nanoparticles Using Copper Ions. *Microchim. Acta* **2015**, *182*, 113–117.
- (17) Baron, R.; Zayats, M.; Willner, I. Dopamine-, L-DOPA-, Adrenaline-, and Noradrenaline-Induced Growth of Au Nanoparticles: Assays for the Detection of Neurotransmitters and of Tyrosinase Activity. *Anal. Chem.* **2005**, *77*, 1566–1571.
- (18) Pem, B.; Toma, M.; Vrček, V.; Vrček, I. V. Combined NMR and Computational Study of Cysteine Oxidation during Nucleation of Metallic Clusters in Biological Systems. *Inorg. Chem.* **2021**, *60*, 4144–4161.
- (19) Gilbert, K. E. *Pcmodel 10.0*; Serena Software: Bloomington, IN, 2014.
- (20) “KICK” stochastic search procedure code. Faculty of Pharmacy and Biochemistry, University of Zagreb <https://kick.science/KICK.html> (accessed 2022-02-01).
- (21) Frisch, M. J.; Trucks, G. W.; Schlegel, H. B.; Scuseria, G. E.; Robb, M. A.; Cheeseman, J. R.; Scalmani, G.; Barone, V.; Petersson, G. A.; Nakatsuji, H.; Li, X.; Caricato, M.; Marenich, A. V.; Bloino, J.; Janesko, B. G.; Gomperts, R.; Mennucci, B.; Hratchian, H. P.; Ortiz, J. V.; Izmaylov, A. F.; Sonnenberg, J. L.; Williams, D. F.; Lipparini, F.; Egidi, F.; Goings, J.; Peng, B.; Petrone, A.; Henderson, T.; Ranasinghe, D.; Zakrzewski, V. G.; Gao, J.; Rega, N.; Zheng, G.; Liang, W.; Hada, M.; Ehara, M.; Toyota, K.; Fukuda, R.; Hasegawa, J.; Ishida, M.; Nakajima, T.; Honda, Y.; Kitao, O.; Nakai, H.; Vreven, T.; Throssell, K.; Montgomery, J. A., Jr.; Peralta, J. E.; Ogliaro, F.; Bearpark, M. J.; Heyd, J. J.; Brothers, E. N.; Kudin, K. N.; Staroverov, V. N.; Keith, T. A.; Kobayashi, R.; Normand, J.; Raghavachari, K.; Rendell, A. P.; Burant, J. C.; Iyengar, S. S.; Tomasi, J.; Cossi, M.; Millam, J. M.; Klene, M.; Adamo, C.; Cammi, R.; Ochterski, J. W.; Martin, R. L.; Morokuma, K.; Farkas, O.; Foresman, J. B.; Fox, D. J. *Gaussian 16*, Revision C.01; Gaussian Inc.: Wallingford, CT, 2016.
- (22) Dennington, R.; Keith, T. A.; Millam, J. M. *GaussView*; SemicheM Inc.: Shawnee Mission, KS, 2016.
- (23) Marenich, A. V.; Cramer, C. J.; Truhlar, D. G. Universal Solvation Model Based on Solute Electron Density and on a Continuum Model of the Solvent Defined by the Bulk Dielectric Constant and Atomic Surface Tensions. *J. Phys. Chem. B* **2009**, *113*, 6378–6396.
- (24) Fukui, K. The Path of Chemical Reactions - the IRC Approach. *Acc. Chem. Res.* **1981**, *14*, 363–368.
- (25) Hratchian, H. P.; Schlegel, H. B. Using Hessian Updating To Increase the Efficiency of a Hessian Based Predictor-Corrector

Reaction Path Following Method. *J. Chem. Theory Comput.* **2005**, *1*, 61–69.

(26) Case, D. A.; Belfon, K.; Ben-Shalom, I. Y.; Brozell, S. R.; Cerutti, D. S.; Cheatham, T. E., III; Cruzeiro, V. W. D.; Darden, T. A.; Duke, R. E.; Giambasu, G.; Gilson, M. K.; Gohlke, H.; Goetz, A. W.; Harris, R.; Izadi, S.; Izmailov, S. A.; Kasavajhala, K.; Kovalenko, A.; Krasny, R.; Kurtzman, T.; Lee, T. S.; LeGrand, S.; Li, P.; Lin, C.; Liu, J.; Luchko, T.; Luo, R.; Man, V.; Merz, K. M.; Miao, Y.; Mikhailovskii, O.; Monard, G.; Nguyen, H.; Onufriev, A.; Pan, F.; Pantano, S.; Qi, R.; Roe, D. R.; Roitberg, A.; Sagui, C.; Schott-Verdugo, S.; Shen, J.; Simmerling, C. L.; Skrynnikov, N. R.; Smith, J.; Swails, J.; Walker, R. C.; Wang, J.; Wilson, L.; Wolf, R. M.; Wu, X.; Xiong, Y.; Xue, Y.; York, D. M.; Kollman, P. A. *AMBER 2017*; University of California: San Francisco, 2017.

(27) Heinz, H.; Vaia, R. A.; Farmer, B. L.; Naik, R. R. Accurate Simulation of Surfaces and Interfaces of Face-Centered Cubic Metals Using 12–6 and 9–6 Lennard-Jones Potentials. *J. Phys. Chem. C* **2008**, *112*, 17281–17290.

(28) Yu, J.; Becker, M. L.; Carri, G. A. The Influence of Amino Acid Sequence and Functionality on the Binding Process of Peptides onto Gold Surfaces. *Langmuir* **2012**, *28*, 1408–1417.

(29) Contreras, M. L.; Torres, C.; Villarroel, I.; Rozas, R. Molecular Dynamics Assessment of Doxorubicin-Carbon Nanotubes Molecular Interactions for the Design of Drug Delivery Systems. *Struct. Chem.* **2019**, *30*, 369–384.

(30) Torres, C.; Villarroel, I.; Rozas, R.; Contreras, L. Carbon Nanotubes Having Haecelkite Defects as Potential Drug Carriers. Molecular Dynamics Simulation. *Molecules* **2019**, *24*, 4281.

(31) Humphrey, W.; Dalke, A.; Schulten, K. VMD - Visual Molecular Dynamics. *J. Mol. Graph.* **1996**, *14*, 33–38.

(32) Siegel, A. L.; Baker, G. A. Bespoke Nanostars: Synthetic Strategies, Tactics, and Uses of Tailored Branched Gold Nanoparticles. *Nanoscale Adv.* **2021**, *3*, 3980–4004.

(33) Wang, X.; Yang, D. P.; Huang, P.; Li, M.; Li, C.; Chen, D.; Cui, D. Hierarchically Assembled Au Microspheres and Sea Urchin-like Architectures: Formation Mechanism and SERS Study. *Nanoscale* **2012**, *4*, 7766–7772.

(34) Qiu, P.; Mao, C. Seed-Mediated Shape Evolution of Gold Nanomaterials: From Spherical Nanoparticles to Polycrystalline Nanochains and Single-Crystalline Nanowires. *J. Nanoparticle Res.* **2009**, *11*, 885–894.

(35) Koeppl, S.; Ghielmetti, N.; Caseri, W.; Spolenak, R. Seed-Mediated Synthesis of Gold Nanorods: Control of the Aspect Ratio by Variation of the Reducing Agent. *J. Nanoparticle Res.* **2013**, *15*, 1471.

(36) Darienzo, R. E.; Mironava, T.; Tannenbaum, R. Raman Signal Enhancement by Quasi-Fractal Geometries of Au Nanoparticles. *J. Nanosci. Nanotechnol.* **2019**, *19*, 4740–4746.

(37) Zhang, X.; Han, Y.; Xing, Z.; Huang, Z.; Xie, R.; Yang, W. Bovine Serum Albumin Assisted Preparation of Ultra-Stable Gold Nanoflowers and Their Selective Raman Response to Charged Dyes. *RSC Adv.* **2019**, *9*, 28228–28233.

(38) Haiss, W.; Thanh, N. T. K.; Aveyard, J.; Fernig, D. G. Determination of Size and Concentration of Gold Nanoparticles from UV-Vis Spectra. *Anal. Chem.* **2007**, *79*, 4215–4221.

(39) Vanderkooy, A.; Chen, Y.; Gonzaga, F.; Brook, M. A. Silica Shell/Gold Core Nanoparticles: Correlating Shell Thickness with the Plasmonic Red-Shift upon Aggregation. *ACS Appl. Mater. Interfaces* **2011**, *3*, 3942–3947.

(40) Bisaglia, M.; Mammi, S.; Bubacco, L. Kinetic and Structural Analysis of the Early Oxidation Products of Dopamine: Analysis of the Interactions with  $\alpha$ -Synuclein. *J. Biol. Chem.* **2007**, *282*, 15597–15605.

(41) Herlinger, E.; Jameson, R. F.; Linert, W. Spontaneous Autoxidation of Dopamine. *J. Chem. Soc. Perkin Trans. 2* **1995**, *2*, 259.

(42) Bernsmann, F.; Ball, V.; Addiego, F.; Ponche, A.; Michel, M.; Gracio, J. J. d. A.; Toniazzo, V.; Ruch, D. Dopamine-Melanin Film Deposition Depends on the Used Oxidant and Buffer Solution. *Langmuir* **2011**, *27*, 2819–2825.

(43) Bacil, R. P.; Chen, L.; Serrano, S. H. P.; Compton, R. G. Dopamine Oxidation at Gold Electrodes: Mechanism and Kinetics near Neutral PH. *Phys. Chem. Chem. Phys.* **2020**, *22*, 607–614.

(44) Madrakian, T.; Afkhami, A.; Borazjani, M.; Bahram, M. Simultaneous Derivative Spectrophotometric Determination of Levodopa and Carbidopa in Pharmaceutical Preparations. *Bull. Korean Chem. Soc.* **2004**, *25*, 1764–1768.

(45) Omotani, H.; Yasuda, M.; Ishii, R.; Ikarashi, T.; Fukuuchi, T.; Yamaoka, N.; Mawatari, K. I.; Kaneko, K.; Nakagomi, K. Analysis of L-DOPA-Derived Melanin and a Novel Degradation Product Formed under Alkaline Conditions. *J. Pharm. Biomed. Anal.* **2016**, *125*, 22–26.

(46) Salomäki, M.; Marttila, L.; Kivelä, H.; Ovinen, T.; Lukkari, J. Effects of PH and Oxidants on the First Steps of Polydopamine Formation: A Thermodynamic Approach. *J. Phys. Chem. B* **2018**, *122*, 6314–6327.

(47) Yang, J.; Cohen Stuart, M. A.; Kamperman, M. Jack of All Trades: Versatile Catechol Crosslinking Mechanisms. *Chem. Soc. Rev.* **2014**, *43*, 8271–8298.

(48) Umek, N.; Geršak, B.; Vintar, N.; Šoštarčič, M.; Mavri, J. Dopamine Autoxidation Is Controlled by Acidic PH. *Front. Mol. Neurosci.* **2018**, *11*, 1–8.

(49) Wang, Y.; Zhang, H.; Chen, M. A Strategy to Differentiate Dopamine and Levodopa Based on Their Cyclization Reaction Regulated by PH. *Anal. Chim. Acta* **2021**, *1157*, 338379.

(50) Zhang, X. P.; Sun, W.; Cao, S. H.; Jiang, W. L.; Peng, H.; Cai, S. H.; Chen, Z. NMR Spectroelectrochemistry in Studies of Dopamine Oxidation. *Electrochemistry* **2020**, *88*, 200–204.

(51) Zheng, W.; Fan, H.; Wang, L.; Jin, Z. Oxidative Self-Polymerization of Dopamine in an Acidic Environment. *Langmuir* **2015**, *31*, 11671–11677.

(52) Chen, T. P.; Liu, T.; Su, T. L.; Liang, J. Self-Polymerization of Dopamine in Acidic Environments without Oxygen. *Langmuir* **2017**, *33*, 5863–5871.

(53) Zhou, Y. Z.; Alany, R. G.; Chuang, V.; Wen, J. Studies of the Rate Constant of L-DOPA Oxidation and Decarboxylation by HPLC. *Chromatographia* **2012**, *75*, 597–606.

(54) Hawley, M. D.; Tatawawadi, S. V.; Piekarski, S.; Adams, R. N. Electrochemical Studies of the Oxidation Pathways of Catecholamines. *J. Am. Chem. Soc.* **1967**, *89*, 447–450.

(55) Young, T. E.; Babbitt, B. W.; Wolfe, L. A. Melanin. 2. Electrochemical Study of the Oxidation of  $\alpha$ -Methyl-dopa and 5,6-Dihydroxy-2-Methylindole. *J. Org. Chem.* **1980**, *45*, 2899–2902.

(56) Young, T.; Babbitt, B. Electrochemical Study of the Oxidation of  $\alpha$ -Methyl-dopamine,  $\alpha$ -Methyl-nor-Adrenaline, and Dopamine. *J. Org. Chem.* **1983**, *48*, 5414.

(57) Hollingsworth, S. A.; Dror, R. O. Molecular Dynamics Simulation for All. *Neuron* **2018**, *99*, 1129–1143.

(58) Mateo-Martí, E.; Rogero, C.; Gonzalez, C.; Sobrado, J. M.; de Andrés, P. L.; Martín-Gago, J. A. Interplay between Fast Diffusion and Molecular Interaction in the Formation of Self-Assembled Nanostructures of S-Cysteine on Au(111). *Langmuir* **2010**, *26*, 4113–4118.

(59) Monti, S.; Carravetta, V.; Ågren, H. Decoration of Gold Nanoparticles with Cysteine in Solution: Reactive Molecular Dynamics Simulations. *Nanoscale* **2016**, *8*, 12929–12938.

(60) Yan, L.; Chen, H.; Jing, C. TiO<sub>2</sub> Facets Shaped by Concentration-Dependent Surface Diffusion of Dopamine. *J. Phys. Chem. Lett.* **2019**, *10*, 898–903.

(61) Hou, T.; Wang, J.; Li, Y.; Wang, W. Assessing the Performance of the MM\_PBSA and MM\_GBSA Methods. 1. The Accuracy. *PDF. J. Chem. Inf. Model* **2011**, *51*, 69–82.

(62) Isabella Cluster. Computing Centre SRCE; University of Zagreb: <https://www.srce.unizg.hr/en/isabella-cluster> (accessed 2002-06-20).